Nano Research Energy

ISSN 2791-0091 (print); 2790-8119 (online)
https://doi.org/10.26599/NRE.2023.9120044

Mini Review

Reviewing the impact of halides on electrochemical CO_2 reduction

Zebi Zhao[1], Jiguang Zhang[2], Ming Lei[1] (✉), and Yanwei Lum[2] (✉)

[1] *State Key Laboratory of Information Photonics and Optical Communications & School of Integrated Circuits, Beijing University of Posts and Telecommunications, Beijing 100876, China*

[2] *Institute of Materials Research and Engineering, Agency for Science, Technology and Research (A*STAR), 2 Fusionopolis way, Innovis, Singapore 138634, Singapore*

Received: 10 October 2022 / **Revised:** 31 October 2022 / **Accepted:** 5 November 2022

ABSTRACT

Electrochemical CO_2 reduction reaction (CO_2RR) is a promising technology for mitigating global warming and storing renewable energy. Designing low-cost and efficient electrocatalysts with high selectivity is a priority to facilitate CO_2 conversion. Halide ion (F^-, Cl^-, Br^-, I^-) modified electrocatalysts is a potential strategy to promote CO_2 reduction and suppress the competitive hydrogen evolution reaction (HER). Therefore, a comprehensive review of the role and mechanism of halide ions in the CO_2RR process can help better guide the future design of efficient electrocatalysts. In this review, we first discuss the role of halide ions on the structure and morphology of electrocatalysts. Secondly, the relationship between the halide ions and the valence states of the active sites on the catalyst surface is further elaborated on. Thirdly, the mechanisms of halide in enhancing CO_2 conversion efficiency are also summarized, including the involvement of halide ions in electron transfer and their influence on the reaction pathway. Finally, we conclude with a summary and future outlook.

KEYWORDS

energy conversion, CO_2 reduction reaction, electrocatalysts, halide ions, catalytic mechanism

1 Introduction

The excessive consumption of fossil fuels has resulted in significant anthropogenic CO_2 emissions, leading to rising temperatures due to the global warming effect [1–3]. Hence, there has been increasing interest in using renewable energy to produce carbon-neutral fuels for the establishment of an artificial carbon cycle [4–6]. One promising way to do this is through electrocatalytic CO_2 reduction reaction (CO_2RR), which uses renewable electricity to convert CO_2 into valuable chemicals and fuels such as carbon monoxide, methane, methanol, formate and ethanol [7–9].

Despite the potential of CO_2RR, its technological implementation is still limited by catalyst activity and selectivity, system efficiency, and understanding of reaction pathways [10–14]. The stable chemical bonding in the CO_2 molecule often results in slow reaction kinetics. In order to drive the conversion of CO_2 to value-added carbon products, CO_2RR has to overcome the high energy barrier of CO_2 activation [15, 16]. Furthermore, the occurrence of other side reactions at the same potential, such as the hydrogen evolution reaction (HER), competes with the reduction of CO_2, which leads to a significant reduction in the selectivity and efficiency of CO_2 reduction [17–20]. Therefore, the development of an electrocatalyst with high activity and selectivity is vital for the practical application of CO_2 electroreduction technology.

Metal-based catalysts have been studied extensively for CO_2RR and the pure metals have been classified into four categories according to the products [3, 21, 22]. Metals such as Au, Ag, Zn, Pd and Ga are highly selective for CO, while Pb, Hg, In, Sn, Cd and Ti are more inclined to produce $HCOO^-$. Copper-based systems, on the other hand, are the only catalysts capable of producing multi-carbon (C_2/C_3) products. Pt, Ti, Ni and Fe are inactive towards CO_2RR and therefore exhibit HER exclusively in aqueous solution [10, 23]. The high overpotentials required for CO_2RR and the simultaneous formation of multiple possible products lead to high energy consumption and low production efficiency [24]. Therefore, modification of metal-based electrocatalysts to inhibit the occurrence of side reactions and improve the selectivity and activity of CO_2RR has been of significant interest.

In this regard, halide ions can potentially modulate the geometry and electronic structure of metal-based electrocatalysts, which is conducive towards optimizing the adsorption and desorption properties of the active sites towards CO_2RR reaction intermediates, thus enhancing the activity and selectivity of catalysts for CO_2RR products and inhibiting HER [25, 26].

Several studies have shown how halide ions can be used for enhancement of electrocatalysts, by stabilizing the active species, regulating the adsorption and desorption of reaction intermediates, reducing the overpotential or participating in the construction of electrocatalyst structures to enhance

Address correspondence to Ming Lei, mlei@bupt.edu.cn; Yanwei Lum, Lum_Yanwei@imre.a-star.edu.sg

activity and selectivity for multi-carbon products [16, 27]. In addition, the presence of halides can reduce the overpotential for the reduction of CO_2. This has been reasoned to be due to halide ions providing electrons to the empty orbitals of CO_2 [28]. After gaining electrons, linear CO_2 converts to the active bent CO_2^{*-} intermediate, leading to more favorable subsequent proton-coupling and electron-transfer steps [29, 30]. Therefore, it has become important to understand the effect of halide ions on metal surfaces and the operating mechanisms at play.

The purpose of this review is to summarize recent advances in understanding the structure and performance of halide modified CO_2RR electrocatalysts. Firstly, the role of halides on structure and morphology of metal-based catalysts is discussed. Secondly, the effect of halide ions on the oxidation state of the catalyst is covered. In addition, the mechanism of how halides contribute to the catalytic conversion of CO_2 is further elaborated on, where the involvement of halide ions in optimizing electron transfer and reaction pathways are presented. Finally, we provide an outlook on use of halides to design highly selective and stable electrocatalysts for CO_2RR.

2 Aspects of halogenated elements affecting the CO_2RR

2.1 The role of halides on structure & morphology

2.1.1 *Halide constructed electrodes*

The use of halide ions to modulate the catalyst structure has become an important strategy to improve the CO_2RR performance. For example, the combination of carbon materials with halides can lead to a change in the geometric structure of carbon compared to pristine carbon materials, resulting in significant catalytic activity towards CO_2RR [31–33]. As shown in Fig. 1, Ni et al. successfully prepared fluorine-doped caged porous carbon (F-CPC), which exhibits a Faradaic efficiency of 88.3% for CO at –1.0 V (vs. RHE) with a current density of –37.5 mA·cm^{-2}. The edge positions of the microporous structure of F-doped carbon shells can generate high electric fields and reduce the thermodynamic energy barrier of CO_2RR, which helps facilitate the conversion of CO_2 to CO [34].

In addition, the specific adsorption properties of halide ions can significantly increase the electrochemical active surface area (ECSA) of the electrode. One reason is that the presence of halides can induce the formation of an ordered and closely packed structural layer of specifically adsorbed ions on the metal surface, which results in much greater coverage of halide ions on the metal surface [35–38]. For example, bismuth oxyiodides are composed of [Bi_xO_y] layers interleaved with iodide [I_z] layers via van der Waals forces, which are unique layered structures with excellent electrical properties [39]. Wang et al. systematically investigated the effect of iodine content on the performance of CO_2RR to formate by regulating the ratio of oxygen to iodine in bismuth oxy-iodide nanosheets. As iodide accelerates the activation of reactants and/or intermediates, the synergistic effect of bismuth and iodide is further enhanced, allowing the Bi_5O_7I catalyst to exhibit an excellent formate Faradaic efficiency of 89% with a partial current density of –13.2 mA·cm^{-2} at –0.89 V vs. RHE [40].

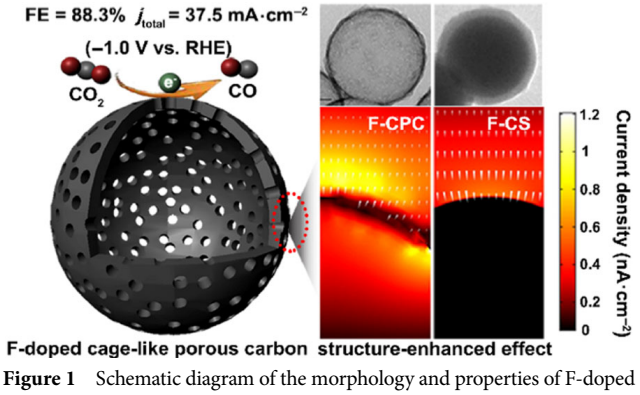

Figure 1 Schematic diagram of the morphology and properties of F-doped cage-like carbon catalyst. Reproduced with permission from Ref. [34], © American Chemical Society 2020.

Halide ions can also influence the conversion process of CO_2 on Ag or Au catalyst surfaces [41–44]. Liu et al. synthesized Ag nanowires (NWs) with diameters less than 25 (D-25) and 100 nm (D-100) by a bromide-mediated method. Compared to D-100 Ag NWs and Ag nanoparticles (NPs), D-25 Ag NWs exhibit higher CO Faradaic efficiency (99.3%) and energy efficiency (61.3%) over a wide potential range. The bromide participates in the formation of this unique nanostructure with an increased edge-to-edge ratio of Ag nanowires, thus enhancing CO_2 electroconversion [45].

Surface Cl^- modification of Ag nanoparticles (Ag-Cl NPs) by *in situ* electroreduction is performed by Fu et al. The Faradaic efficiency of Ag-Cl NPs for CO production reached 98% at –0.8 V vs. RHE. The strong interaction between surface Cl^- ions and CO_2 molecules not only makes the catalysts significantly more efficient for CO_2 capture, but also accelerates the electron transfer from Cl^- ions to CO_2 and promotes the formation of CO_2^{*-} intermediates for the reaction [46].

A strategy for the preparation of Br^- ion adsorbed porous Ag nanowire films (BD-Ag) by electroreduction is also reported by Qiu et al. This strategy involves anodic oxidation of commercial Ag foils and subsequent electrochemical reduction. BD-Ag catalysts can act as efficient electrocatalysts for CO_2 to CO with a high CO Faradaic efficiency of 96.2% at –0.6 vs. RHE in 0.5 M $KHCO_3$. They found that the rate-determining step for the occurrence of CO_2RR in polycrystalline Ag foil is the electron transfer to CO_2 to form CO_2^{*-} intermediates. BD-Ag with surface adsorbed Br^- has lower energy barrier in the rate determining step occurring compared to Ag foil [47].

In addition, researchers have also investigated halide ion constructed multi-metal catalysts [24, 48, 49]. The interaction of the two phases of the tandem AgI-CuO catalyst was investigated by Yang et al., which exhibited a 68.9% C_{2+} Faradaic efficiency. During the electrochemical reduction process, iodide ions leached from the catalyst and inhibited the reduction of CuO, resulting in Cu^0/Cu^+ active sites which promoted the C-C coupling [50].

2.1.2 *Halide derived electrodes*

Metal halide catalysts can be synthesized using the electro-derivative method, typically involving the electrochemical anodic treatment of the electrode in the electrolyte to which halide ions are added [26, 51–57]. As shown in Fig. 2, Kim et al. successfully prepared copper halide derived catalysts using the anodic halogenation method. CuCl, CuBr or CuI surfaces were formed during the halogenation of copper foil in KCl, KBr or KI solutions, respectively. Due to the different properties of the anions, the formation of triangle-based pyramids on the surface of the copper electrode was found only in the sample

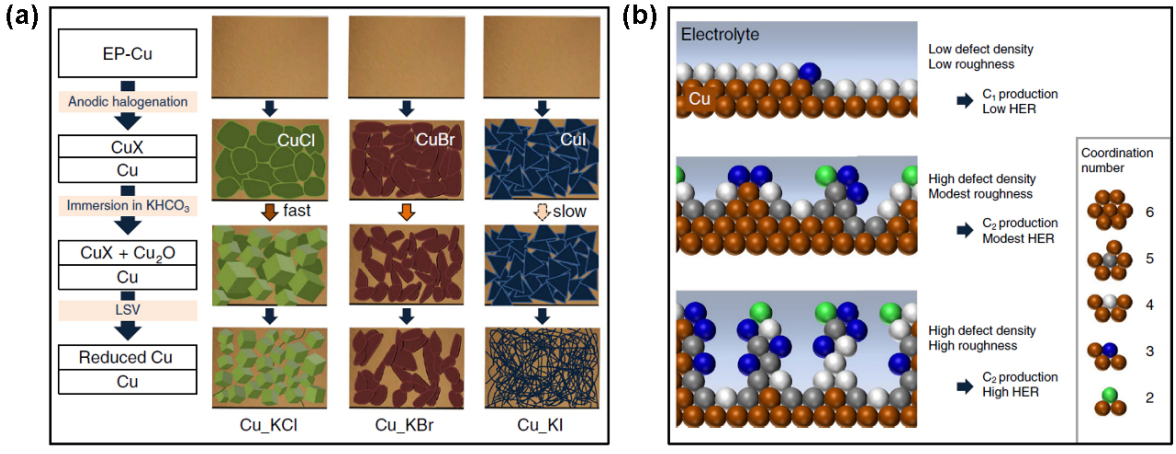

Figure 2 Schematic diagram of the synthesis process and morphology of electro-derived Cu-based catalysts. (a) Schematic diagram of the anodic halogenated synthesis. (b) Active sites coordination and two-dimensional visualization and corresponding results in the CO_2RR process. Reproduced with permission from Ref. [7], © Kim, T. et al. 2020.

treated with KI. In the subsequent oxidation/reduction cycles, the copper halide on the surface was gradually transformed to metallic copper, with the surface of the copper foil accumulating a large number of defects. The defects were proposed to act as active sites to promote the C-C coupling reaction, thus enhancing the efficient conversion of CO_2 to C_{2+} products [7].

Kwon et al. exploited the adsorption properties of halide to modify the copper nanostructure and subsequently found that this can lead to catalysts with higher selectivity towards C_{2+} products such as ethylene and ethanol. Cl^- ions in the electrolyte can effectively stabilize the Cu (100) crystal plane and promote the formation of nanocubic Cu_2O particles. The formation of C_{2+} products at a lower overpotential than methane is favored when CO_2RR occurs on Cu (100) surfaces. Thus, exposed and stable Cu (100) greatly contribute to improved ethylene/ethanol selectivity and higher ethylene to methane ratio (C_2H_4/CH_4) [58].

Porous Ag nanowires (Ag NWs) with high electrochemical surface area were prepared by electroreduction of AgCl nanowires by Park et al. It is shown that the large electrochemical surface area of Ag nanowires, which is 90 times larger than that of Ag films, along with Ag^+ facilitate the conversion of CO_2 to CO, leading the CO Faradaic efficiency up to 98.7% while the current density of Ag NWs reaches -3.16 mA·cm^{-2} at -0.8 vs. RHE [59].

Additionally, researchers have found that using halide electroderivatization techniques can modulate specific favorable crystalline surfaces, active sites and oxidation states in the catalysts, thus enhancing the efficiency of CO_2 to formate conversion [60–64]. For example, Arquer et al. proposed a strategy to produce bismuth nanosheets using bismuth oxy-bromide. The preferential exposure of highly active bismuth crystal planes promotes CO_2 conversion to formate, with a Faradaic efficiency of more than 90% at -200 mA·cm^{-2} [25]. Han et al. found that bismuth oxy-iodide nanosheets can be topologically transformed into ultrathin bismuth nanosheets. Due to the single-crystal bismuth and the expanded surface area, the electrocatalyst possesses >90% formate selectivity within a wide potential range with good stability at high current density for 10 h. The full-cell energy conversion efficiency of this system can reach up to 47% [65].

Halides can also be converted to new compounds during the oxidation/reduction cycles to improve the efficiency towards CO_2RR. Huang et al. first prepared PbF_2 nanoclusters with an average size of 3 nm using a low-temperature solution method. Subsequently, PbF_2 was induced to reconstitute to $Pb_3(CO_3)_2(OH)_2$ in a CO_2-saturated environment. The reconstituted catalyst exhibited high selectivity to formate, with Faradaic efficiency of 90.1% at -1.2 V vs. RHE. Additionally, the authors further doped $Pb_3(CO_3)_2(OH)_2$ with Pd (4 wt.%) to enhance its adsorption to HCO_3^- and thus accelerate CO_2 protonation. The Pd-$Pb_3(CO_3)_2(OH)_2$ (4 wt.%) reaches a maximum formate Faradaic efficiency of 96.5% at -1.2 V vs. RHE with a current density of around -13 mA·cm^{-2} [66].

A novel Cu-Pd heterostructure (Cu-Pd-c3), derived from CuCl-PdO_x hexagonal microplates, was prepared by Xie et al. for CH_4 production from electrochemical CO_2 reduction. CuCl-PdO_x hexagonal microplates were synthesized by a dual-potential electrodeposition technique, followed by electrochemical reduction to form Cu-Pd heterostructures. Compared with pure Cu or Pd, the hollow sites in the Pd region of the Cu-Pd heterostructure can stabilize the CO* intermediate and selectively lower the overpotential for CH_4 formation. Cu-Pd-c3 catalyst can effectively electroreduce CO_2 to CH_4, maintaining the Faradaic efficiency of CH_4 above 30% at -1.2 to -1.25 V vs. RHE [67].

2.2 The role of halides on electronic structure

Although halide ions contribute significantly to assist in catalyst surface reorganization, this is not the only way to enhance the activity and selectivity of CO_2RR by halide ions. Halide modulation of the oxidation state of the electrocatalyst is also an effective strategy to improve the performance [68]. In the CO_2RR process, the oxidation state of the catalyst active site determines the ease of CO_2 activation and reaction intermediate uptake and desorption, which directly affects the product selectivity [69, 70].

The relationship between halide anions and oxidation state in zinc-based catalysts was investigated by Nguyen et al. They found that the adsorption of halide ions on the electrode surface greatly enhanced the catalytic activity. The current density of the electrode increased with the trend of F < Cl < Br < I, which is relative to the increase in adsorption strength from F^- to I^-. The adsorption of halide ions makes the oxidation state of Zn increase and the formation of highly oxidized Zn species in the nanoporous Zn-catalyst promotes the protonation

of CO_2 and stabilizes the subsequently formed COOH* intermediate, resulting in a Faradaic efficiency of up to 97% for CO [71].

It is known that the oxidation state of Cu is important for CO_2RR to C_2 products [72, 73]. Kibria et al. used surface reconstruction to modulate the valence state of the active site on the catalyst surface. During a wet oxidation process, the copper surface is first partially oxidized to form an initial copper chloride layer and subsequently converted to a cuprous oxide surface. This method allows the CO_2RR to shift away from CH_4 and towards C_{2+} products. It is speculated that after the activation of CO_2, the catalyst provides strong adsorption sites for CO* intermediates to promote the C-C coupling reaction, thus improving the selectivity towards C_{2+} products [74].

Moreover, previous studies have shown that the high oxidation state of Sn is key to achieving high activity for CO_2RR to formate due to the optimal adsorption energy towards CO_2^{*-} and HCOO* intermediates [75]. However, the negative reduction potential applied to Sn-based electrocatalysts during CO_2RR causes the reduction of Sn species with high oxidation states, which diminishes the catalytic activity. This phenomenon can be suppressed in an alkaline electrolyte (Fig. 3). However, due to the presence of CO_2, the alkaline electrolyte is gradually neutralized. Therefore, ensuring that Sn-based electrocatalysts maintain a high oxidation state at high current densities is important [28]. Ko et al. investigated fluorine-doped tin oxide catalysts for CO_2RR to formic acid. *In-situ* spectroscopy shows that the fluorine-modified tin-based electrocatalyst maintains a high oxidation state of Sn at negative reduction potentials. Fluorine doping not only enhances the interactions between $HCOO^-$ and catalyst surface but also alters electronic structure of CO_2 to facilitate electron transfer. The fluorine doped tin oxide exhibited higher performance compared to conventional tin oxide catalysts, achieving a high current density (–330 mA·cm^{-2}) and high Faradaic efficiency (95% at –100 mA·cm^{-2}) for the production of formate [28].

Halide ions can also change the charge distribution on the catalyst surface to alter the oxidation state of the active site, for example by elevating the surface oxygen vacancy concentration [76]. Zhu et al. reported the synthesis of bilayer-$Bi_{12}O_{17}Cl_2$ nanosheets (BBNs) with abundant oxygen-rich vacancies using a hydrothermal method. The abundant oxygen vacancies provide more active sites for BBNs while promoting ion transport and electrical conductivity. BBNs exhibit good activity, selectivity and stability during CO_2 electroreduction. The Faradaic efficiency of formate reaches >92% at –0.89 V vs. RHE with a current density of –11.5 mA·cm^{-2}, remaining stable for 12 h continuous operation [77].

Li et al. also used fluorine to replace the oxygen site and successfully prepared the chalcogenide fluorine oxide $Sr_2Fe_{1.5}Mo_{0.5}O_{6-\delta}F_{0.1}$ (F-SFM). The good conductivity of this mixed ion material promotes the adsorption and dissociation of CO_2, which can be attributed to the fluorine doping increasing the oxygen vacancy concentration and decreasing the polarization resistance at the reaction interface, thus accelerating the formation of CO_2^{*-} [78, 79].

It is proposed that when halide ions approach the metal surface, these can accelerate the further conversion of key intermediates in CO_2RR, thus enhancing the efficiency of CO_2 conversion [16]. In addition, the synergistic effect of halide and specific active sites can inhibit the activation and dissociation of H_2O, thus stabilizing the activated CO_2 molecules. A good example is the synergistic interaction of halides with organic substances [80]. Wang et al. designed and synthesized crystalline single-chain models (Cu-PzH, Cu-PzCl, Cu-PzBr, and Cu-PzI) to study the selectivity of CO_2 electroreduction products. The main structural differences between Cu-PzH, Cu-PzCl, Cu-PzBr and Cu-PzI are the substituents of the halogen atoms with different electronegativity on the pyrazole

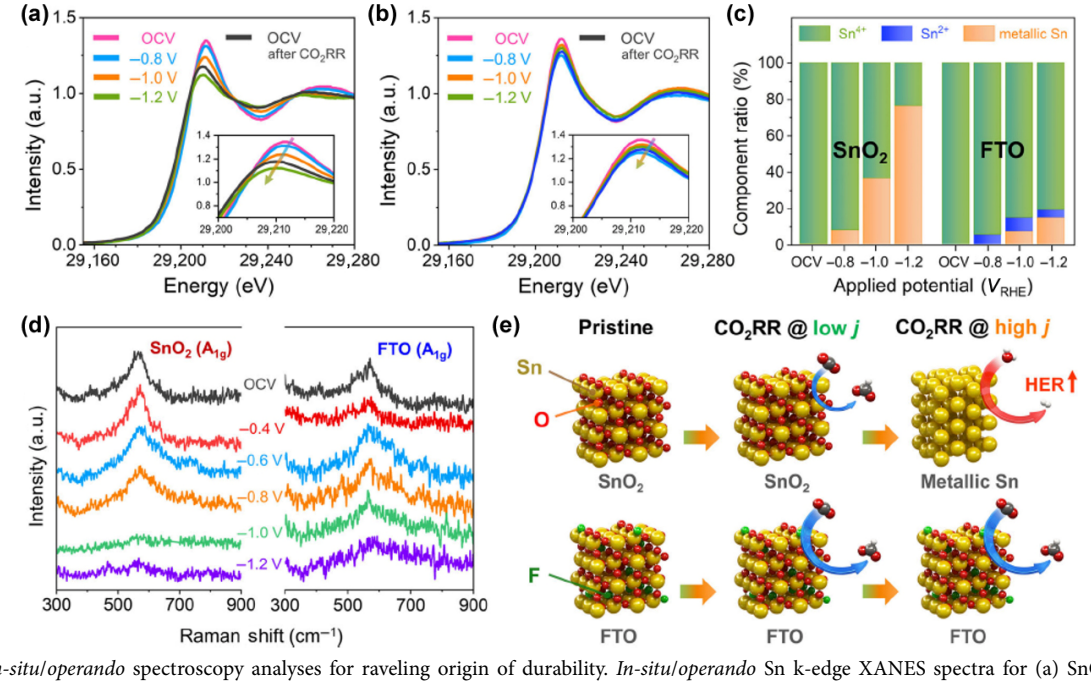

Figure 3 *In-situ/operando* spectroscopy analyses for raveling origin of durability. *In-situ/operando* Sn k-edge XANES spectra for (a) SnO_2/C and (b) FTO/C catalysts during CO_2RR in the flow-type electrolyzer and (c) its oxidation state distribution deconvoluted by linear combination fitting (orange: Sn, blue: Sn^{2+}, and green: Sn^{4+}). (d) *In-situ/operando* SER spectra obtained at constant potentials for SnO_2 and FTO catalysts without carbon supporter. Analyzed SER spectra present in the wavenumber region of 300–900 cm^{-1}. (e) Schematic illustration of reaction affinity for SnO_2 and FTO under low/high cathodic overpotential. Reproduced with permission from Ref. [28], © Ko, Y. J. et al. 2022.

ligands. The selectivity of CH_4 increases when the substituent of the ligand changes from Cl to Br to I. Cu-PzI has the highest CH_4 Faradaic efficiency (54%) at –1.0 V vs. RHE with a large current density of –287.52 mA·cm^{-2}. The synergistic effect (D_{Cu-Cu} and β_{Cu-Cu}) between neighboring catalytic active sites induced by the variation of the coordination microenvironment changes the distance of C-C coupling. Furthermore, the d-band center of copper is upshifted from the Fermi energy level due to the polarization of halogen, which leads to an increase in the binding strength of Cu sites and *HCO, resulting in a better selectivity for CH_4 [81].

Wang et al. constructed a metal-molecule interface doped with halide ions to generate ethanol. Experimental results show that the co-involvement of dodecanethiol with copper bromide resulted in a high Faradaic efficiency of 72% for C_{2+} products. The high selectivity is attributed to the anion-modulated metal-molecule electrocatalyst interface. Theoretical calculations show that the Br^- species stabilize high-valence copper species in the electrode and modulate the adsorption energy of key intermediates at the reaction interface, thus facilitating the selective conversion of CO_2 to ethanol [82].

The adsorption of halide ions on the surface of Ag electrode decreased its Fermi energy level, creating a new active site: X-Ag$_n^+$ [83]. Li et al. reported a study on the modification of Ag electrode surface valence states by trace amounts of bromide ions. It is shown that the residual bromide ions in the system are adsorbed onto the electrode surface. The charge redistribution increases the number of metal sites providing electrons for the conversion of CO_2 to CO. Moreover, the modulation of the metal valence on the catalyst surface inhibits the adsorption of protons and therefore suppresses the evolution of hydrogen. The modified electrode achieves a CO Faradaic efficiency of 77.8% at –0.6 V (vs. RHE) [84].

The active sites at the edge of the catalyst and those at the basal plane can exhibit different catalytic activities [85, 86]. This is due to the different coordination environment at the edge of the catalyst compared to the bulk [87]. Lv et al. found that the edge molybdenum atoms in molybdenum disulfide could be modified with fluorine elements to enhance the binding energy to CO* intermediates. As a result, fluorosilane (FAS)-modified MoS_2 nanosheets (H-E-MoS_2) exhibit excellent CO_2 reduction performance. The Faradaic efficiency of H-E-MoS_2 for CO production reached 81.2% at –0.9 V vs. RHE [88].

Single-atom catalysts modulate the charge distribution of metal atoms by changing the surrounding environment compared to the bulk metal [89]. The most typical structures are the M-N_4 sites (M is a metal element), and their electronic structure can be further modulated by halogens in order to promote the desorption of CO* and inhibit the adsorption of H* [90]. In the study by Han et al., fluorine-tuned nickel-based single-atom catalysts were successfully prepared by polymer-assisted pyrolysis. Figure 4 illustrates F doping changing the electronic configuration of the Ni-N_4 site, lowering the energy barrier for CO_2 activation, and facilitating the generation of the key *COOH intermediate. As a result, the electroreduction of CO_2 to CO can be effectively achieved over Ni-SAs@FNC catalysts, maintaining the Faradaic efficiency of CO over 95% at –0.67 to –0.97 V vs. RHE, which is better than the undoped case [91]. Kong et al. also found that halide ions contribute to the transfer of electrons from the transition metal d orbitals of cobalt-based monatomic catalysts to the unoccupied π orbitals of CO_2. Theoretical calculations showed that halides, especially

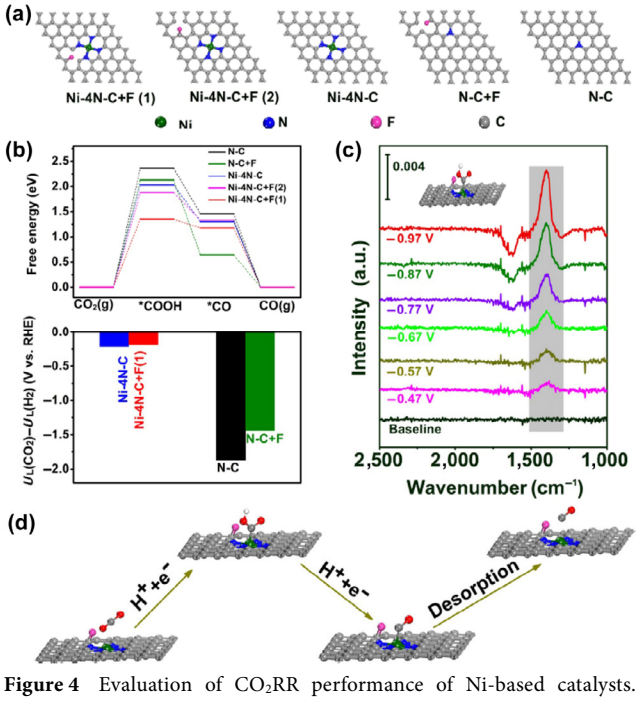

Figure 4 Evaluation of CO_2RR performance of Ni-based catalysts. (a) Different model structures of the catalysts, (b) calculated Gibbs free energy diagrams for CO_2-to-CO conversion on different catalysts, (c) the difference between the calculated limiting potentials for CO_2 reduction and H_2 evolution, (d) *in situ* ATR-IR spectra collected under different applied potentials in CO_2-saturated 0.5M $KHCO_3$ and (e) the proposed reaction pathways of CO_2RR over Ni-SAs@FNC. Reproduced permission from Ref. [91], © Elsevier B. V. 2020.

bromide ions, excited the high spin state of 3d electrons in cobalt ions. The reaction energy barrier for the formation of CO is correspondingly lowered due to the facilitation of CO_2 activation brought by the high spin state, thus the cobalt-based monatomic catalysts exhibit a high selectivity for CO. The high spin state percentage of 65.6% for the bromine-doped cobalt-based molecules (Co-salophen-Br) exceeds the chloride and iodide ion-modified electrocatalysts. Thus Co-salophen-Br is able to exhibit 98.5% CO selectivity at –0.70 V vs. RHE [29, 92].

2.3 The role of halides as direct promoters

The first step in CO_2RR is the activation of CO_2 and this involves the transfer of an electron to the empty orbital of the CO_2 molecule, which results in a CO_2^{*-} radical intermediate [93–95]. Lee et al. investigated the effect of different halogen-containing functional group polymer binders on enhancing the CO_2RR performance of Au-based catalysts. The authors incorporated various binders with different key functional groups onto Au electrodes respectively using a co-precipitation method. It is shown that a gold electrode containing fluorine functional groups (Au(111)-CF_2) can be used for CO_2RR to CO with a maximum Faradaic efficiency of 94.7%. The authors suggest that the reason for the high CO selectivity of the catalyst is that the halide ions adsorb and stabilize the *COOH intermediates. Notably, these polymers weaken the hydrogen adsorption on the Au surface, which provides more active sites for CO_2RR intermediates [96].

In addition to modifying the binding energy of the active sites, halide ions can also modulate the charge distribution of CO* intermediates. The halides adsorbed on the metal surface

cause local charge redistribution, resulting in the carbon atom of adsorbed CO* to become positively charged [97, 98]. On the contrary, when *CO is adsorbed onto a non-halide surface, the C side is negatively charged. The two carbon atoms with opposite charges are closely linked by strong electrostatic attraction, thus facilitating the C-C coupling process [99, 100].

Huang et al. investigated the effect of different electrolyte aqueous solutions (0.1 M $KClO_4$, KCl, KBr and KI) on the electroreduction reaction of CO_2 on Cu (100) and Cu (111) surfaces. The halide ions play a critical role in enhancing the formation of C_2 products, by tuning the coordination environment of adsorbed *CO for more efficient C-C coupling. The amount of *CO on the Cu surface increases as the electrolyte anion changes from ClO_4^- to Cl^- to Br^- to I^-. The formation rate of ethylene and ethanol on Cu (100) and Cu (111) surfaces increased as the electrolyte anion was changed from $ClO_4^- \rightarrow Cl^- \rightarrow Br^- \rightarrow I^-$. This trend mirrors that of the binding strength of the anions on Cu in the order of $ClO_4^- < Cl^- < Br^- < I^-$. The total Faradaic efficiency for C_2 and C_3 products was as high as 74% at –1.23 V vs. RHE in the KI electrolyte [101].

Changing the active site adsorption mode by adjusting the halide coverage on the electrode surface is one of the strategies to improve the CO_2 reduction performance [102–104]. Garg et al. reported the different halide ions in the electrolyte affect the conversion of CO_2 to CO on Ag electrode. With the weakening adsorption strength of halide ions on the Ag surface ($I^-<Br^-<Cl^-$), the activity for CO_2RR to CO is enhanced. The iodide ion-modified Ag electrode achieves 97% CO selectivity at –1.3 V vs. RHE. This is due to the weakly attached halide ions that facilitate the conversion of CO_2 to *COOH intermediates, thus accelerating CO production [105]. Theoretical calculations illustrate that the interactions between adsorbed species can also indirectly affect the binding strength of intermediates on the surface interface [106, 107]. Cho et al. found that functionalizing Au electrodes with CN^- and Cl^- was able to increase the CO Faradaic efficiency from 20% to 80%. This is due to van der Waals interactions from the two anions stabilizing *COOH and lowering the energy barrier for CO_2RR to CO [108].

Previous studies have shown that halogenated elements on metal surfaces play an important role in activating water molecules. The interaction with hydrated cations enhances the electronegativity of the halide, thus accelerating the process of H_2O activation and dissociation [109]. Ma et al. performed a systematic study on the C-C coupling mechanism of hydrogen-assisted halogen-modified copper catalysts. Figure 5 reveals that the fluoride ion on the Cu surface accelerates the hydrogenation of *CO to *CHO, reducing the Gibbs free energy of *CHO formation by 0.31 eV. *CHO then undergoes C-C coupling, resulting in C_{2+} product formation. A high current density of –1,600 $mA \cdot cm^{-2}$ was achieved at –0.89 V vs. RHE, and the selectivity of C_{2+} products reached 80% [4].

In addition, halide ions can facilitate electron transfer to the empty orbitals of CO_2 [110, 111]. Theoretical calculations show that the Fermi energy level of CO_2 is 3.8 eV, which corresponds to the electron affinity of CO_2 [112]. The electron affinity of F_2 is the largest among the halogenated elements, and the value of corresponding Fermi energy level is 3.0 eV, which is smaller than that of CO_2. The high electron affinity indicates that electrons tend to transfer to the empty orbitals of CO_2 from halide ions [113]. Ogura et al. reported the effect of halide ions adsorbed on the surface of copper electrodes on enhancing the performance of CO_2RR. The different electron affinities allow halides to act as ligands to facilitate electron transfer to CO_2. The halide ions and CO_2 are attracted and tightly bound to each other, thus forming X_{ad}-C bonds. The formation of X_{ad}-C bonds facilitates the electron transfer from electrode to CO_2 while inhibiting HER. Therefore, the bonding of halide to CO_2 can significantly reduce the overpotential and enhance the CO_2 reduction activity [111].

Varela et al. showed that the influence of halide ions on the

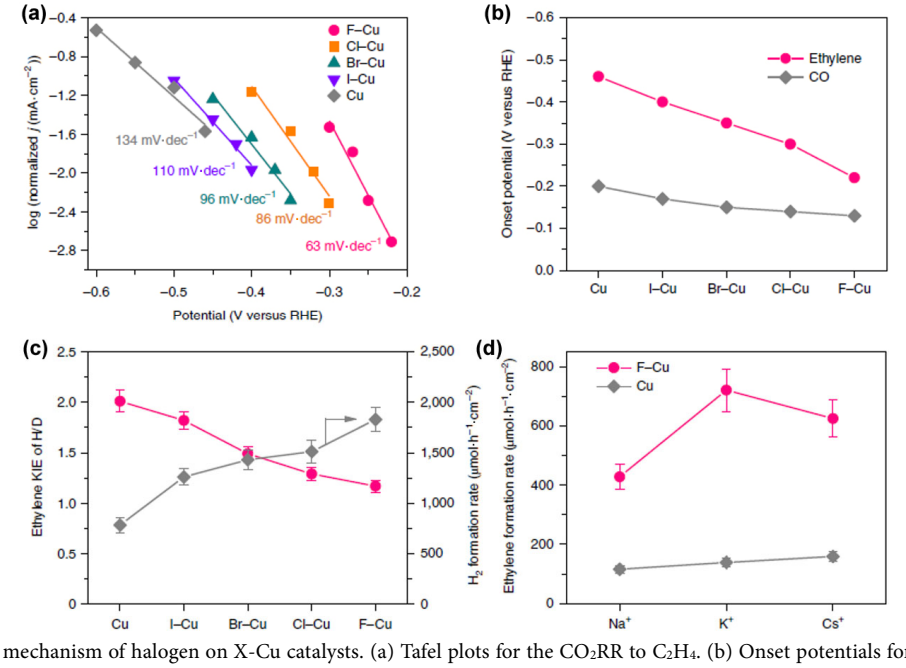

Figure 5 Functioning mechanism of halogen on X-Cu catalysts. (a) Tafel plots for the CO_2RR to C_2H_4. (b) Onset potentials for CO and C_2H_4. (c) KIE of H/D in CO_2RR to ethylene and hydrogen evolution performance under an argon atmosphere at –0.6 V vs. RHE. (d) Effect of alkali metal cations in MOH (M = Na^+, K^+ and Cs^+) electrolyte on CO_2RR to C_2H_4 at –0.6 V vs. RHE over copper and F-Cu catalysts. Reproduced with permission from Ref. [4], © Ma, W. C. et al., under exclusive licence to Springer Nature Limited 2020.

CO_2RR process depends on the properties of the halide ions and their concentration. Some studies have shown that it is easier to convert CO_2 to CO on copper surfaces with the help of Cl^- or Br^-. However, the presence of I^- facilitates the formation of methane. The rate of methane production at I^- modified copper electrodes is 5 times higher than pristine copper electrodes at –0.9 V vs. RHE. The electronegetivity of I^- ions is weaker than that of Cl^- or Br^-, thus facilitating electron transfer to the metal surface from adsorbed I^- and reducing the difficulty of CO protonation. The ease of CO protonation often determines the ease of CH_4 formation [114].

The strong interaction created by the halide adsorption on the metal surface with the reactants accelerates the CO_2RR process. The accelerated reaction consumes a large number of protons around the electrode surface, resulting in a high local pH around the electrode-electrolyte interface, which is favorable for C-C coupling and suppresses HER [115–118]. In addition, the role of deep eutectic solvents containing halogenated elements in CO_2RR was systematically investigated by Ahmad et al. Due to the high alkalinity, polarity and dielectric constant of the deep eutectic solvents, the system has a significantly enhanced ability to dissolve CO_2 molecules, thus enhancing mass transfer. The CO Faradaic efficiency of the Ag electrode reaches 71% at –1.1 V vs. RHE [119].

3 Summary and outlook

CO_2RR is important due to its ability to achieve both CO_2 utilization and storage of renewable energy. To do so, it is necessary to further enhance the catalyst activity as well as the selectivity for specific carbon products (Tables 1 and 2). In this review, we summarize the effect of halides on CO_2RR. Various methods of halide modification of electrocatalyst surfaces and structures are presented, which can be categorized into two types: halide constructed electrodes and halide derived electrodes. Halides can also influence the selectivity of specific products by modulating and stabilizing the electronic structure of the active sites to accelerate CO_2 activation and modulate the binding strength of reaction intermediates. Moreover, halide ions could also participate in the reaction as direct promoters. Furthermore, theoretical calculations and experimental results show that halides could directly affect the binding strength and reaction path of the intermediates. For example, halogenated elements can accelerate the hydrogenation of CO* to CHO* on the catalyst surface, thereby accelerating C-C coupling and improving the selectivity of C_{2+} products.

Despite substantial progress about halide influence on electrochemical CO_2 reduction, we highlight three topical areas that still warrant in-depth investigation and research.

(1) Design model systems to identify key mechanisms in different situations

We have classified mechanisms by which halides contribute to electrochemical CO_2 reduction under nanostructure reorganization, modulation of electronic structure, and direct promotion. However, these factors could all impact the catalyst simultaneously, which makes it difficult to distinguish the key ones at play. The coexistence and potential synergy of multiple mechanisms can also hinder our attempts at understanding the key mechanisms that promote CO_2 conversion. Therefore, to gain insight into the role of halide ions in CO_2 reduction reactions, it is necessary to systematically design well-defined model systems to study the key mechanisms for each case. Some examples of potential candidate model systems are as follows:

Firstly, various single crystal surfaces could be prepared and tested in different halide containing electrolytes to obtain clearer catalyst structure-halide interaction correlations. Secondly, current electrochemical methods for preparing halide-derived catalysts inevitably create high surface area structures. To eliminate these surface area/morphology effects and better

Table 1 Comparison of electrochemical performance of various copper-based catalysts for C_{2+} products

Catalyst	Electrolyte	Applied potential	Current density ($mA \cdot cm^{-2}$)	Cell type	Faradaic efficiency	Reference
F-Cu	0.75 M KOH	–0.89 V vs. RHE	–1,600	Flow cell	65.2% (Ethylene)	[4]
Cu_KBr	0.1 M $KHCO_3$	–1.15 V vs. RHE	–42.7	H-cell	49.5% (Ethylene)	[7]
Cu_3-Br	0.5 M KOH	–0.70 V vs. RHE	–129.58	Flow cell	55.01%	[35]
Cu-CuI electrode	1 M KOH	–0.87 V vs. RHE	–550	Flow cell	~35 % (Ethylene)	[48]
CuO-FEP	1.0 M KOH	–0.80 V vs. RHE	–8	H-cell	15% (Ethylene)	[49]
AgI-CuO	0.25 M $KHCO_3$	–1.00 V vs. RHE	–25	H-cell	~50% (Ethylene)	[50]
2F-Cu-BDC derived catalyst	1 M KOH	–1.65 V vs. RHE	–150	Flow cell	40% (Ethylene)	[53]
Cu NFs (I)	0.1 M $KHCO_3$	–0.735 V vs. RHE	–20	H-cell	30% (C_2H_6)	[54]
Cu_I	0.1 M $KHCO_3$	–0.90 V vs. RHE	–31.2	H-cell	80% (C_{2+} products)	[55]
CuOHFCl NSs	0.1 M $KHCO_3$	–1.00 V vs. RHE	–15	H-cell	53.8% (C_{2+} products)	[56]
Cu/Cu_xOF	1 M KOH	–0.30 V vs. RHE	–4	Flow cell	27% (CH_3COO^-)	[70]
Cu_2O/ILGS-x	0.1 M $KHCO_3$	–1.10 V vs. RHE	–123.1	Flow cell	39.4% (Ethanol)	[79]
N2-500	0.1 M $KHCO_3$+0.1 M KI	–1.70 V vs. RHE	–33	H-cell	37.2% (Ethylene)	[80]
Cu-PzH	1 M KOH	–1.00 V vs. RHE	–346.46	Flow cell	60% (Ethylene)	[81]
CuBr-DDT	0.5 M KCl	–1.25 V vs. RHE	–8.75	H-cell	35.9% (Ethanol)	[82]
Cu@PIL-F-1.2	3 M KOH	–0.75 V vs. RHE	–174	Flow cell	58% (C_{2+} products)	[93]
Cu (100)	0.1 M KI	–1.23 V vs. RHE	–12.06	H-cell	50% (Ethylene)	[101]
BIF-102NSs	0.5 M $KHCO_3$	–1.00 V vs. RHE	–14	H-cell	11.3% (Ethylene)	[117]
K-F-Cu-CO_2	1 M KOH	–0.53 vs. RHE	–800	Flow cell	52.9% (Ethanol)	[123]

Table 2 Comparison of electrochemical performance of various catalysts for formate or CO products

Catalyst	Electrolyte	Applied potential	Current density ($mA \cdot cm^{-2}$)	Cell type	Faradaic efficiency	Reference
BiOBr-templated catalysts	0.1 M $KHCO_3$	–1.00 V vs. RHE	–80	H-cell	99% (Formate)	[25]
FTO/C	1 M KOH	–0.50 V vs. RHE	–100	Flow cell	95% (Formate)	[28]
Co-salophen-Br	0.5 M $KHCO_3$	–0.70 V vs. RHE	–17.5	H-cell	98.5% (CO)	[29]
NF-C-950	0.1 M $KHCO_3$	–0.60 V vs. RHE	–2	H-cell	90% (CO)	[31]
FC	0.1 M $KHCO_3$	–0.62 V vs. RHE	–0.224	H-cell	89.6% (CO)	[33]
F-CPC	0.5 M $KHCO_3$	–1.00 V vs. RHE	–37.5	H-cell	88.3% (CO)	[34]
$BiOCl_{0.5}Br_{0.5}$	0.5 M $KHCO_3$	–1.60 V vs. SCE	–9.7	H-cell	98.4% (Formate)	[39]
Bi_5O_7I	0.5 M $KHCO_3$	–0.89 V vs. RHE	–14.9	H-cell	89.0% (Formate)	[40]
P-SGDEs	0.5 M $KHCO_3$	–1.80 V vs. Ag/AgCl	–21.67	H-cell	86.75% (Formate)	[42]
Ag-Cl NP	0.5 M $KHCO_3$	–0.80 V vs. RHE	–9.4	H-cell	98% (CO)	[46]
BD-Ag	0.5 M $KHCO_3$	–0.60 V vs. RHE	–15	H-cell	96.2% (CO)	[47]
Ag NWs	0.1 M $KHCO_3$	–0.80 V vs. RHE	–3.6	H-cell	98.7% (Formate)	[59]
Bi PNS	0.5 M $KHCO_3$	–1.40 V vs. RHE	–72	Flow cell	95.2% (Formate)	[60]
POD-Bi	0.5 M $KHCO_3$	–1.16 V vs. RHE	–57	H-cell	95% (Formate)	[61]
BiOI	0.5 M $KHCO_3$	–0.90 V vs. RHE	–31.1	H-cell	97.1% (Formate)	[63]
BiNS	0.5 M $NaHCO_3$	–1.50 V vs. SCE	–14	H-cell	~100% (Formate)	[65]
$Pb_3(CO_3)_2(OH)_2$	0.1 M $KHCO_3$	–1.20 V vs. RHE	–9.5	H-cell	90.1% (Formate)	[66]
FNC-SnOF	0.1 M $KHCO_3$	–0.75 V vs. RHE	–10	H-cell	95.2% (CO)	[75]
BiOI-Bi NSs	0.5 M $KHCO_3$	–1.00 V vs. RHE	–50	H-cell	91.33 % (Formate)	[76]
BBNs	0.5 M $NaHCO_3$	–0.89 V vs. RHE	–11.5	H-cell	93.5 % (Formate)	[77]
Br-Ag	Supersaturated NH_4HCO_3	–0.50 V vs. RHE	~–10	H-cell	74.0% (CO)	[83]
Br-Ag(OR)	Saturated NH_4HCO_3	–0.60 V vs. RHE	–13.8	H-cell	77.8% (CO)	[84]
H-E-MoS_2	EmimBF_4/water	–0.90 V vs. RHE	–31	H-cell	81.2% (CO)	[88]
FeN_4Cl/NC	0.5 M $KHCO_3$	–0.60 V vs. RHE	–9.78	H-cell	90.5% (CO)	[89]
Ni-SAs@FNC	0.5 M $KHCO_3$	–0.77 V vs. RHE	–25	H-cell	95% (CO)	[91]
Ga/C-CP	0.1 M Bu_4NCl/AN	–2.50 V vs. Ag/AgCl	–14.5	H-cell	84% (CO)	[95]
CADF Indium	0.5 M $KHCO_3$	–0.86 V vs. RHE	~ –10	H-cell	86% (Formate)	[98]
Ag electrode	0.1 M KI + 0.1 M $KHCO_3$	–0.99 V vs. RHE	–23.71	H-cell	90.3% (CO)	[104]
Ag foils	0.1 M ChI	–1.30 V vs RHE	~ –5.5	H-cell	97% (CO)	[105]
Au sputtered electrode	0.25 M KCl + 0.25 M $KHCO_3$	–0.70 V vs. RHE	~ –5	H-cell	82% (CO)	[106]
Gallium electrode	0.1 M Bu_4NCl/AN	–2.40 V vs. RHE	–10	H-cell	83% (CO)	[112]
CoPc based GDEs	1 M KOH	–3.50 V vs. Hg/HgO	–110	Flow cell	99.2% (CO)	[115]
Bi dendrite	1 M $KHCO_3$ + 0.1 M CsCl	–0.85 V vs. RHE	–13.8	H-cell	~100% (Formate)	[120]
OMP-Ni-N-C	2.0 M KCl	–0.60 V vs. RHE	–3	H-cell	99% (CO)	[121]
CoPc/g-C_3N_4	0.6 M NaCl+0.6 M $NaHCO_3$	–1.40 V vs. Ag/AgCl	–16	H-cell	89.5% (CO)	[122]

understand the role of halides, flat halide thin films could be grown and used as catalysts for CO_2 reduction. In addition, such systems could be more amenable to depth-profiling analysis. Thirdly, metal halide catalysts are inherently unstable under reaction conditions. To circumvent this issue, halide-doped carbon materials could be employed as the substrate, in order to host small metal nanoparticulate (e.g., 5 nm) catalysts to better study the role of halides.

(2) Develop advanced *in-situ* characterization tools to understand the role of halides

Under reaction conditions, the catalyst surface structure, active sites, valence state and reaction intermediates could be dynamically changing. However, such dynamic changes often occur for extremely short periods, and the role of halogenated elements in the reaction process may not be fully reflected by *ex-situ* characterization studies. Therefore, advanced *in-situ* characterization techniques and methods for measuring catalyst surface and structure changes should be used. For example, *in-situ* X-ray absorption spectroscopy (XAS) could be used to study the oxidation state of the catalyst under reaction conditions. *In-situ* transmission electron microscopy (TEM) could be used to observe how the nanostructure of the catalyst changes during CO_2 reduction.

(3) Explore new halide-based catalyst architectures

Up to now, the focus has been on the development of halide modified metal-based electrocatalysts. Beyond such systems, there may be other opportunities for design of new types of electrocatalysts. For example, doping of halogens into carbon-based catalysts and using organic halide compounds as molecular additives to enhance electrocatalytic activity could become new highly promising avenues for exploration [29, 43, 81, 89–92].

Acknowledgements

This study was supported financially by the Fundamental Research Funds for the Central Universities (2021XD-A04-2) and the Fund of State Key Laboratory of Information Photonics and Optical Communications (Beijing University of Posts and Telecommunications, P.R. China). Additionally, Zebi Zhao acknowledges the financial assistance from China Scholarship Council (CSC, No. 202206470057). Y. L. acknowledges support and funding from A*STAR Career Development Award (Project No. 202D800037).

Declaration of conflicting interests

The authors declare no conflicting interests regarding the content of this article.

References

[1] Huang, J. E.; Li, F. W.; Ozden, A.; Rasouli, A. S.; De Arquer, F. P. G.; Liu, S. J.; Zhang, S. Z.; Luo, M. C.; Wang, X.; Lum, Y. et al. CO_2 electrolysis to multicarbon products in strong acid. *Science* **2021**, *372*, 1074–1078.

[2] Dinh, C. T.; Burdyny, T.; Kibria, M. G.; Seifitokaldani, A.; Gabardo, C. M.; De Arquer, F. P. G.; Kiani, A.; Edwards, J. P.; De Luna, P.; Bushuyev, O. S. et al. CO_2 electroreduction to ethylene via hydroxide-mediated copper catalysis at an abrupt interface. *Science* **2018**, *360*, 783–787.

[3] Lum, Y.; Ager, J. W. Evidence for product-specific active sites on oxide-derived Cu catalysts for electrochemical CO_2 reduction. *Nat. Catal.* **2019**, *2*, 86–93.

[4] Ma, W. C.; Xie, S. J.; Liu, T. T.; Fan, Q. Y.; Ye, J. Y.; Sun, F. F.; Jiang, Z.; Zhang, Q. H.; Cheng, J.; Wang, Y. Electrocatalytic reduction of CO_2 to ethylene and ethanol through hydrogen-assisted C-C coupling over fluorine-modified copper. *Nat. Catal.* **2020**, *3*, 478–487.

[5] Lum, Y.; Cheng, T.; Goddard III, W. A.; Ager, J. W. Electrochemical CO reduction builds solvent water into oxygenate products. *J. Am. Chem. Soc.* **2018**, *140*, 9337–9340.

[6] Ding, N.; Lum, Y.; Chen, S. F.; Chien, S. W.; Hor, T. S. A.; Liu, Z. L.; Zong, Y. Sulfur-carbon yolk-shell particle based 3D interconnected nanostructures as cathodes for rechargeable lithium-sulfur batteries. *J. Mater. Chem. A* **2015**, *3*, 1853–1857.

[7] Kim, T.; Palmore, G. T. R. A scalable method for preparing Cu electrocatalysts that convert CO_2 into C_{2+} products. *Nat. Commun.* **2020**, *11*, 3622.

[8] Singh, M. R.; Kwon, Y.; Lum, Y.; Ager III, J. W.; Bell, A. T. Hydrolysis of electrolyte cations enhances the electrochemical reduction of CO_2 over Ag and Cu. *J. Am. Chem. Soc.* **2016**, *138*, 13006–13012.

[9] Lum, Y.; Huang, J. E.; Wang, Z. Y.; Luo, M. C.; Nam, D. H.; Leow, W. R.; Chen, B.; Wicks, J.; Li, Y. C.; Wang, Y. H. et al. Tuning OH binding energy enables selective electrochemical oxidation of ethylene to ethylene glycol. *Nat. Catal.* **2020**, *3*, 14–22.

[10] Nitopi, S.; Bertheussen, E.; Scott, S. B.; Liu, X. Y.; Engstfeld, A. K.; Horch, S.; Seger, B.; Stephens, I. E. L.; Chan, K.; Hahn, C. et al. Progress and perspectives of electrochemical CO_2 reduction on copper in aqueous electrolyte. *Chem. Rev.* **2019**, *119*, 7610–7672.

[11] He, J. F.; Wu, C. H.; Li, Y. M.; Li, C. L. Design of pre-catalysts for heterogeneous CO_2 electrochemical reduction. *J. Mater. Chem. A* **2021**, *9*, 19508–19533.

[12] Lai, W. C.; Ma, Z. S.; Zhang, J. W.; Yuan, Y. L.; Qiao, Y.; Huang, H. Dynamic evolution of active sites in electrocatalytic CO_2 reduction reaction: Fundamental understanding and recent progress. *Adv. Funct. Mater.* **2022**, *32*, 2111193.

[13] Lai, W. C.; Qiao, Y.; Zhang, J. W.; Lin, Z. Q.; Huang, H. W. Design strategies for markedly enhancing energy efficiency in the electrocatalytic CO_2 reduction reaction. *Energy Environ. Sci.* **2022**, *15*, 3603–3629.

[14] Zhang, J. W.; Zeng, G. M.; Chen, L. L.; Lai, W. C.; Yuan, Y. L.; Lu, Y. F.; Ma, C.; Zhang, W. H.; Huang, H. W. Tuning the reaction path of CO_2 electroreduction reaction on indium single-atom catalyst: Insights into the active sites. *Nano Res.* **2022**, *15*, 4014–4022.

[15] Eid, K.; Lu, Q. Q.; Abdel-Azeim, S.; Soliman, A.; Abdullah, A. M.; Abdelgwad, A. M.; Forbes, R. P.; Ozoemena, K. I.; Varma, R. S.; Shibl, M. F. Highly exfoliated $Ti_3C_2T_x$ MXene nanosheets atomically doped with Cu for efficient electrochemical CO_2 reduction: An experimental and theoretical study. *J. Mater. Chem. A* **2022**, *10*, 1965–1975.

[16] Masana, J. J.; Peng, B. W.; Shuai, Z. Y.; Qiu, M.; Yu, Y. Influence of halide ions on the electrochemical reduction of carbon dioxide over a copper surface. *J. Mater. Chem. A* **2022**, *10*, 1086–1104.

[17] Halilu, A.; Hayyan, M.; Aroua, M. K.; Yusoff, R.; Hizaddin, H. F. Mechanistic insights into carbon dioxide utilization by superoxide ion generated electrochemically in ionic liquid electrolyte. *Phys. Chem. Chem. Phys.* **2021**, *23*, 1114–1126.

[18] Kiss, A. A.; Pragt, J. J.; Vos, H. J.; Bargeman, G.; De Groot, M. T. Novel efficient process for methanol synthesis by CO_2 hydrogenation. *Chem. Eng. J.* **2016**, *284*, 260–269.

[19] Luo, S. H.; Zeng, Z. T.; Wang, H.; Xiong, W. P.; Song, B.; Zhou, C. Y.; Duan, A. B.; Tan, X. F.; He, Q. Y.; Zeng, G. M. et al. Recent progress in conjugated microporous polymers for clean energy: Synthesis, modification, computer simulations, and applications. *Progr. Polym. Sci.* **2021**, *115*, 101374.

[20] Wu, Y. Z.; Cao, S. Y.; Hou, J. G.; Li, Z. W.; Zhang, B.; Zhai, P. L.; Zhang, Y. T.; Sun, L. C. Rational design of nanocatalysts with nonmetal species modification for electrochemical CO_2 reduction. *Adv. Energy Mater.* **2020**, *10*, 2000588.

[21] Pérez-Sequera, A. C.; Díaz-Pérez, M. A.; Serrano-Ruiz, J. C. Recent advances in the electroreduction of CO_2 over heteroatom-doped carbon materials. *Catalysts* **2020**, *10*, 1179.

[22] Li, H.; Jiang, T. W.; Qin, X. X.; Chen, J.; Ma, X. Y.; Jiang, K.; Zhang, X. G.; Cai, W. B. Selective reduction of CO_2 to CO on an Sb-modified Cu electrode: Spontaneous fabrication and physical insight. *ACS Catal.* **2021**, *11*, 6846–6856.

[23] Lum, Y.; Ager, J. W. Sequential catalysis controls selectivity in electrochemical CO_2 reduction on Cu. *Energy Environ. Sci.* **2018**, *11*, 2935–2944.

[24] Lamaison, S.; Wakerley, D.; Kracke, F.; Moore, T.; Zhou, L.; Lee, D. U.; Wang, L.; Hubert, M. A.; Acosta, J. E. A.; Gregoire, J. M. et al. Designing a Zn-Ag catalyst matrix and electrolyzer system for CO_2 Conversion to CO and beyond. *Adv. Mater.* **2022**, *34*, e2103963.

[25] De Arquer, F. P. G.; Bushuyev, O. S.; De Luna, P.; Dinh, C. T.; Seifitokaldani, A.; Saidaminov, M. I.; Tan, C. S.; Quan, L. N.; Proppe, A.; Kibria, M. G. et al. 2D metal oxyhalide-derived catalysts for efficient CO_2 electroreduction. *Adv. Mater.* **2018**, *30*, 1802858.

[26] Arán-Ais, R. M.; Rizo, R.; Grosse, P.; Algara-Siller, G.; Dembélé, K.; Plodinec, M.; Lunkenbein, T.; Chee, S. W.; Cuenya, B. R. Imaging electrochemically synthesized Cu_2O cubes and their morphological evolution under conditions relevant to CO_2 electroreduction. *Nat. Commun.* **2020**, *11*, 3489.

[27] Li, S. J.; Dong, X.; Zhao, Y. H.; Mao, J. N.; Chen, W.; Chen, A. H.; Song, Y. F.; Li, G. H.; Jiang, Z.; Wei, W. et al. Chloride ion adsorption enables ampere-level CO_2 electroreduction over silver hollow fiber. *Angew. Chem., Int. Ed.* **2022**, *61*, e202210432.

[28] Ko, Y. J.; Kim, J. Y.; Lee, W. H.; Kim, M. G.; Seong, T. Y.; Park, J.; Jeong, Y.; Min, B. K.; Lee, W. S.; Lee, D. K. et al. Exploring dopant effects in stannic oxide nanoparticles for CO_2 electro-reduction to formate. *Nat. Commun.* **2022**, *13*, 2205.

[29] Kong, X. D.; Ke, J. W.; Wang, Z. Q.; Liu, Y.; Wang, Y. B.; Zhou, W. R.; Yang, Z. W.; Yan, W. S.; Geng, Z. G.; Zeng, J. Co-based molecular catalysts for efficient CO_2 reduction via regulating spin states. *Appl. Catal. B Environ.* **2021**, *290*, 120067.

[30] Varela, A. S.; Kroschel, M.; Reier, T.; Strasser, P. Controlling the selectivity of CO_2 electroreduction on copper: The effect of the electrolyte concentration and the importance of the local pH. *Catal. Today* **2016**, *260*, 8–13.

[31] Pan, F. P.; Li, B. Y.; Xiang, X. M.; Wang, G. F.; Li, Y. Efficient CO_2

electroreduction by highly dense and active pyridinic nitrogen on holey carbon layers with fluorine engineering. *ACS Catal*. **2019**, *9*, 2124–2133.

[32] Wicks, J.; Jue, M. L.; Beck, V. A.; Oakdale, J. S.; Dudukovic, N. A.; Clemens, A. L.; Liang, S. W.; Ellis, M. E.; Lee, G.; Baker, S. E. et al. 3D-printable fluoropolymer gas diffusion layers for CO_2 electroreduction. *Adv*. *Mater*. **2021**, *33*, 2003855.

[33] Xie, J. F.; Zhao, X. T.; Wu, M. X.; Li, Q. H.; Wang, Y. B.; Yao, J. N. Metal-free fluorine-doped carbon electrocatalyst for CO_2 reduction outcompeting hydrogen evolution. *Angew*. *Chem., Int*. *Ed*. **2018**, *57*, 9640–9644.

[34] Ni, W.; Xue, Y. F.; Zang, X. G.; Li, C. X.; Wang, H. Z.; Yang, Z. Y.; Yan, Y. M. Fluorine doped cagelike carbon electrocatalyst: An insight into the structure-enhanced CO selectivity for CO_2 reduction at high overpotential. *ACS Nano* **2020**, *14*, 2014–2023.

[35] Lu, Y. F.; Dong, L. Z.; Liu, J.; Yang, R. X.; Liu, J. J.; Zhang, Y.; Zhang, L.; Wang, Y. R.; Li, S. L.; Lan, Y. Q. Predesign of catalytically active sites via stable coordination cluster model system for electroreduction of CO_2 to ethylene. *Angew*. *Chem., Int*. *Ed*. **2021**, *60*, 26210–26217.

[36] Sheelam, A.; Muneeb, A.; Talukdar, B.; Ravindranath, R.; Huang, S. J.; Kuo, C. H.; Sankar, R. Flexible and free-standing polyvinyl alcohol-reduced graphene oxide-Cu_2O/CuO thin films for electrochemical reduction of carbon dioxide. *J*. *Appl*. *Electrochem*. **2020**, *50*, 979–991.

[37] Grosse, P.; Yoon, A.; Rettenmaier, C.; Chee, S. W.; Cuenya, B. R. Growth dynamics and processes governing the stability of electrodeposited size-controlled cubic Cu catalysts. *J*. *Phys*. *Chem*. *C* **2020**, *124*, 26908–26915.

[38] Ogura, K.; Oohara, R.; Kudo, Y. Reduction of CO_2 to ethylene at three-phase interface effects of electrode substrate and catalytic coating. *J*. *Electrochem*. *Soc*. **2005**, *152*, D213.

[39] Qiu, Y.; Du, J.; Dong, W.; Dai, C. N.; Tao, C. Y. Selective conversion of CO_2 to formate on a size tunable nano-Bi electrocatalyst. *J*. *CO_2 Utilizat*. **2017**, *20*, 328–335.

[40] Wang, Q. Z.; Ma, M.; Zhang, S. S.; Lu, K. K.; Fu, L. J.; Liu, X. J.; Chen, Y. H. Influence of the chemical compositions of bismuth oxyiodides on the electroreduction of carbon dioxide to formate. *ChemPlusChem* **2020**, *85*, 672–678.

[41] Hsieh, Y. C.; Betancourt, L. E.; Senanayake, S. D.; Hu, E. Y.; Zhang, Y.; Xu, W. Q.; Polyansky, D. E. Modification of CO_2 reduction activity of nanostructured silver electrocatalysts by surface halide anions. *ACS Appl*. *Energy Mater*. **2019**, *2*, 102–109.

[42] Wang, Q. N.; Dong, H.; Yu, H.; Yu, H. B. Enhanced performance of gas diffusion electrode for electrochemical reduction of carbon dioxide to formate by adding polytetrafluoroethylene into catalyst layer. *J*. *Power Sources* **2015**, *279*, 1–5.

[43] Wan, X. K.; Wang, J. Q.; Wang, Q. M. Ligand-protected Au_{55} with a novel structure and remarkable CO_2 electroreduction performance. *Angew*. *Chem., Int*. *Ed*. **2021**, *60*, 20748–20753.

[44] Raciti, D.; Braun, T.; Tackett, B. M.; Xu, H.; Cruz, M.; Wiley, B. J.; Moffat, T. P. High-aspect-ratio Ag nanowire mat electrodes for electrochemical CO production from CO_2. *ACS Catal*. **2021**, *11*, 11945–11959.

[45] Liu, S. B.; Wang, X. Z.; Tao, H. B.; Li, T. F.; Liu, Q.; Xu, Z. H.; Fu, X. Z.; Luo, J. L. Ultrathin 5-fold twinned sub-25 nm silver nanowires enable highly selective electroreduction of CO_2 to CO. *Nano Energy* **2018**, *45*, 456–462.

[46] Fu, H. Q.; Zhang, L.; Zheng, L. R.; Liu, P. F.; Zhao, H. J.; Yang, H. G. Enhanced CO_2 electroreduction performance over Cl-modified metal catalysts. *J*. *Mater*. *Chem*. *A* **2019**, *7*, 12420–12425.

[47] Qiu, W. B.; Liang, R. P.; Luo, Y. L.; Cui, G. W.; Qiu, J. D.; Sun, X. P. A Br^- anion adsorbed porous Ag nanowire film: *In situ* electrochemical preparation and application toward efficient CO_2 electroreduction to CO with high selectivity. *Inorg*. *Chem*. *Front*. **2018**, *5*, 2238–2241.

[48] Li, H. F.; Liu, T. F.; Wei, P. F.; Lin, L.; Gao, D. F.; Wang, G. X.; Bao, X. H. High-rate CO_2 electroreduction to C_{2+} products over a copper-copper iodide catalyst. *Angew*. *Chem., Int*. *Ed*. **2021**, *60*, 14329–14333.

[49] Liu, P.; Liu, H. L.; Zhang, S.; Wang, J.; Wang, C. Significant role of reconstructed character on CuO-derived catalyst for enhanced electrocatalytic reduction of CO_2 to multicarbon products. *Electrochim*. *Acta* **2020**, *354*, 136753.

[50] Yang, R. O.; Duan, J. Y.; Dong, P. P.; Wen, Q. L.; Wu, M.; Liu, Y. W.; Liu, Y.; Li, H. Q.; Zhai, T. Y. *In situ* halogen-ion leaching regulates multiple sites on tandem catalysts for efficient CO_2 electroreduction to C_{2+} products. *Angew*. *Chem., Int*. *Ed*. **2022**, *61*, e202116706.

[51] Gao, D. F.; Scholten, F.; Cuenya, B. R. Improved CO_2 electroreduction performance on plasma-activated Cu catalysts via electrolyte design: Halide effect. *ACS Catal*. **2017**, *7*, 5112–5120.

[52] Lee, S.; Kim, D.; Lee, J. Electrocatalytic Production of C_3-C_4 compounds by conversion of CO_2 on a chloride-induced Bi-phasic Cu_2O-Cu catalyst. *Angew*. *Chem., Int*. *Ed*. **2015**, *54*, 14701–14705.

[53] Chen, R. Z.; Cheng, L.; Liu, J. Z.; Wang, Y. T.; Ge, W. X.; Xiao, C. Q.; Jiang, H.; Li, Y. H.; Li, C. Z. Toward high-performance CO_2-to-C_2 electroreduction via linker tuning on MOF-derived catalysts. *Small* **2022**, *18*, 2200720.

[54] Wang, H.; Matios, E.; Wang, C. L.; Luo, J. M.; Lu, X.; Hu, X. F.; Li, W. Y. Rapid and scalable synthesis of cuprous halide-derived copper nano-architectures for selective electrochemical reduction of carbon dioxide. *Nano Lett*. **2019**, *19*, 3925–3932.

[55] Gao, D. F.; Sinev, I.; Scholten, F.; Arán-Ais, R. M.; Divins, N. J.; Kvashnina, K.; Timoshenko, J.; Cuenya, B. R. Selective CO_2 electroreduction to ethylene and multicarbon alcohols via electrolyte-driven nanostructuring. *Angew*. *Chem., Int*. *Ed*. **2019**, *58*, 17047–17053.

[56] Li, M. H.; Ma, Y. Y.; Chen, J.; Lawrence, R.; Luo, W.; Sacchi, M.; Jiang, W.; Yang, J. P. Residual chlorine induced cationic active species on a porous copper electrocatalyst for highly stable electrochemical CO_2 reduction to C_{2+}. *Angew*. *Chem., Int*. *Ed*. **2021**, *60*, 11487–11493.

[57] Yoon, A.; Poon, J.; Grosse, P.; Chee, S. W.; Cuenya, B. R. Iodide-mediated Cu catalyst restructuring during CO_2 electroreduction. *J*. *Mater*. *Chem*. *A* **2022**, *10*, 14041–14050.

[58] Kwon, Y.; Lum, Y.; Clark, E. L.; Ager, J. W.; Bell, A. T. CO_2 electroreduction with enhanced ethylene and ethanol selectivity by nanostructuring polycrystalline copper. *ChemElectroChem* **2016**, *3*, 1012–1019.

[59] Park, J. Y.; Dong, W. J.; Lee, J. L. Monolithic Cl-modified nanoporous Ag nanowires for electrochemical CO_2 reduction to CO. *ACS Appl*. *Energy Mater*. **2022**, *5*, 1627–1634.

[60] Fu, X. B.; Wang, J. A.; Hu, X. B.; He, K.; Tu, Q.; Yue, Q.; Kang, Y. J. Scalable chemical interface confinement reduction BiOBr to bismuth porous nanosheets for electroreduction of carbon dioxide to liquid fuel. *Adv*. *Funct*. *Mater*. **2021**, *32*, 2107182.

[61] He, S. S.; Ni, F. L.; Ji, Y. J.; Wang, L.; Wen, Y. Z.; Bai, H. P.; Liu, G. J.; Zhang, Y.; Li, Y. Y.; Zhang, B. et al. The p-orbital delocalization of main-group metals to boost CO_2 electroreduction. *Angew*. *Chem., Int*. *Ed*. **2018**, *57*, 16114–16119.

[62] Liu, P.; Liu, H. L.; Zhang, S.; Wang, J.; Wang, C. Effects of thicknesses and sizes of BiOX nanoplates precursors on derived Bi nanosheets for efficient CO_2 electroreduction. *J*. *CO_2 Utilizat*. **2021**, *51*, 101643.

[63] Zheng, H. Z.; Wu, G. L.; Gao, G. H.; Wang, X. X. The bismuth architecture assembled by nanotubes used as highly efficient electrocatalyst for CO_2 reduction to formate. *Chem*. *Eng*. *J*. **2021**, *421*, 129606.

[64] Tang, J. M.; Tang, J. B.; Mayyas, M.; Ghasemian, M. B.; Sun, J.; Rahim, M. A.; Yang, J.; Han, J. L.; Lawes, D. J.; Jalili, R. et al. Liquid-metal-enabled mechanical-energy-induced CO_2 conversion. *Adv*. *Mater*. **2022**, *34*, e2105789.

[65] Han, N.; Wang, Y.; Yang, H.; Deng, J.; Wu, J. H.; Li, Y. F.; Li, Y. G. Ultrathin bismuth nanosheets from *in situ* topotactic transformation for selective electrocatalytic CO_2 reduction to formate. *Nat*. *Commun*. **2018**, *9*, 1320.

[66] Huang, W. J.; Wang, Y. J.; Liu, J. W.; Wang, Y.; Liu, D. B.; Dong, J. F.; Jia, N.; Yang, L.; Liu, C. T.; Liu, Z. et al. Efficient and selective CO_2 reduction to formate on Pd-doped $Pb_3(CO_3)_2(OH)_2$: Dynamic

catalyst reconstruction and accelerated CO_2 protonation. *Small* **2022**, *18*, 2107885.

[67] Xie, J. F.; Chen, J. J.; Huang, Y. X.; Zhang, X.; Wang, W. K.; Huang, G. X.; Yu, H. Q. Selective electrochemical CO_2 reduction on Cu-Pd heterostructure. *Appl. Catal. B Environ.* **2020**, *270*, 118864.

[68] Vasileff, A.; Zhu, Y. P.; Zhi, X.; Zhao, Y. Q.; Ge, L.; Chen, H. M.; Zheng, Y.; Qiao, S. Z. Electrochemical reduction of CO_2 to ethane through stabilization of an ethoxy intermediate. *Angew. Chem., Int. Ed.* **2020**, *59*, 19649–19653.

[69] Lum, Y.; Yue, B. B.; Lobaccaro, P.; Bell, A. T.; Ager, J. W. Optimizing C-C coupling on oxide-derived copper catalysts for electrochemical CO_2 reduction. *J. Phys. Chem. C* **2017**, *121*, 14191–14203.

[70] Cai, R. M.; Sun, M. Z.; Ren, J. Z.; Ju, M.; Long, X.; Huang, B. L.; Yang, S. H. Unexpected high selectivity for acetate formation from CO_2 reduction with copper based 2D hybrid catalysts at ultralow potentials. *Chem. Sci.* **2021**, *12*, 15382–15388.

[71] Nguyen, D. L. T.; Jee, M. S.; Won, D. H.; Oh, H. S.; Min, B. K.; Hwang, Y. J. Effect of halides on nanoporous Zn-based catalysts for highly efficient electroreduction of CO_2 to CO. *Catal. Commun.* **2018**, *114*, 109–113.

[72] Li, Y. H.; Xu, A. N.; Lum, Y.; Wang, X.; Hung, S. F.; Chen, B.; Wang, Z. Y.; Xu, Y.; Li, F. W.; Abed, J. et al. Promoting CO_2 methanation via ligand-stabilized metal oxide clusters as hydrogen-donating motifs. *Nat. Commun.* **2020**, *11*, 6190.

[73] Lum, Y.; Ager, J. W. Stability of residual oxides in oxide-derived copper catalysts for electrochemical CO_2 reduction investigated with ^{18}O labeling. *Angew. Chem., Int. Ed.* **2018**, *57*, 551–554.

[74] Kibria, M. G.; Dinh, C. T.; Seifitokaldani, A.; De Luna, P.; Burdyny, T.; Quintero-Bermudez, R.; Ross, M. B.; Bushuyev, O. S.; De Arquer, F. P. G.; Yang, P. D. et al. A Surface reconstruction route to high productivity and selectivity in CO_2 electroreduction toward C_{2+} hydrocarbons. *Adv. Mater.* **2018**, *30*, 1804867.

[75] Ni, W. P.; Gao, Y.; Lin, Y.; Ma, C.; Guo, X. G.; Wang, S. Y.; Zhang, S. G. Nonnitrogen coordination environment steering electrochemical CO_2-to-CO conversion over single-atom tin catalysts in a wide potential window. *ACS Catal.* **2021**, *11*, 5212–5221.

[76] Wang, D.; Wang, Y. Y.; Chang, K.; Zhang, Y. N.; Wang, Z. L.; Zhang, Z. D.; Pan, C. S.; Lou, Y.; Zhu, Y. F.; Zhang, Y. Residual iodine on *in-situ* transformed bismuth nanosheets induced activity difference in CO_2 electroreduction. *J. CO_2 Utilizat.* **2022**, *55*, 101802.

[77] Zhu, J. H.; Fan, J.; Cheng, T. L.; Cao, M. Y.; Sun, Z. H.; Zhou, R.; Huang, L.; Wang, D.; Li, Y. G.; Wu, Y. P. Bilayer nanosheets of unusual stoichiometric bismuth oxychloride for potassium ion storage and CO_2 reduction. *Nano Energy* **2020**, *75*, 104939.

[78] Li, Y. H.; Li, Y.; Wan, Y. H.; Xie, Y.; Zhu, J. F.; Pan, H. B.; Zheng, X. S.; Xia, C. R. Perovskite oxyfluoride electrode enabling direct electrolyzing carbon dioxide with excellent electrochemical performances. *Adv. Energy Mater.* **2019**, *9*, 1803156.

[79] Wang, W. H.; Ma, Z. G.; Fei, X.; Wang, X. S.; Yang, Z. X.; Wang, Y.; Zhang, J. Q.; Ning, H.; Tsubaki, N.; Wu, M. B. Joint tuning the morphology and oxygen vacancy of Cu_2O by ionic liquid enables high-efficient CO_2 reduction to C_2 products. *Chem. Eng. J.* **2022**, *436*, 135029.

[80] Yang, Y.; Li, K. J.; Ajmal, S.; Feng, Y. Q.; Bacha, A. U. R.; Nabi, I.; Zhang, L. W. Interplay between halides in the electrolyte and the chemical states of Cu in Cu-based electrodes determines the selectivity of the C_2 product. *Sustain. Energy Fuels* **2020**, *4*, 2284–2292.

[81] Wang, R.; Liu, J.; Huang, Q.; Dong, L. Z.; Li, S. L.; Lan, Y. Q. Partial coordination-perturbed Bi-copper sites for selective electroreduction of CO_2 to hydrocarbons. *Angew. Chem., Int. Ed.* **2021**, *60*, 19829–19835.

[82] Wang, J. H.; Yang, H.; Liu, Q. Q.; Liu, Q.; Li, X. T.; Lv, X. Z.; Cheng, T.; Wu, H. B. Fastening Br^- ions at copper-molecule interface enables highly efficient electroreduction of CO_2 to ethanol. *ACS Energy Lett.* **2021**, *6*, 437–444.

[83] Li, H. Y.; Gao, J. M.; Shan, J. J.; Du, Q.; Zhang, Y.; Guo, X.; Xie, M.; Wu, S. H.; Wang, Z. J. Effect of halogen-modification on Ag catalyst for CO_2 electrochemical reduction to syngas from NH_4HCO_3 electrolyte. *J. Environ. Chem. Eng.* **2021**, *9*, 106415.

[84] Li, H. Y.; Gao, J. M.; Du, Q.; Shan, J. J.; Zhang, Y.; Wu, S. H.; Wang, Z. J. Direct CO_2 electroreduction from NH_4HCO_3 electrolyte to syngas on bromine-modified Ag catalyst. *Energy* **2021**, *216*, 119250.

[85] Cheng, Y. W.; Xu, X. J.; Li, Y. T.; Zhang, Y. M.; Song, Y. CO_2 reduction mechanism on the Nb_2CO_2 MXene surface: Effect of nonmetal and metal modification. *Computat. Mater. Sci.* **2022**, *202*, 110971.

[86] Zhao, Q.; Zhang, C.; Hu, R. M.; Du, Z. G.; Gu, J. N.; Cui, Y. L. S.; Chen, X.; Xu, W. J.; Cheng, Z. J.; Li, S. M. et al. Selective etching quaternary MAX phase toward single atom copper immobilized MXene ($Ti_3C_2Cl_x$) for efficient CO_2 electroreduction to methanol. *ACS Nano* **2021**, *15*, 4927–4936.

[87] Handoko, A. D.; Chen, H. T.; Lum, Y.; Zhang, Q. F.; Anasori, B.; Seh, Z. W. Two-dimensional titanium and molybdenum carbide MXenes as electrocatalysts for CO_2 reduction. *iScience* **2020**, *23*, 101181.

[88] Lv, K. L.; Teng, C.; Shi, M. H.; Yuan, Y.; Zhu, Y.; Wang, J. R.; Kong, Z.; Lu, X. Y.; Zhu, Y. Hydrophobic and electronic properties of the E-MoS_2 nanosheets induced by FAS for the CO_2 electroreduction to syngas with a wide range of CO/H_2 ratios. *Adv. Funct. Mater.* **2018**, *28*, 1802339.

[89] Li, Z.; Wu, R.; Xiao, S. H.; Yang, Y. C.; Lai, L. O.; Chen, J. S.; Chen, Y. Axial chlorine coordinated iron-nitrogen-carbon single-atom catalysts for efficient electrochemical CO_2 reduction. *Chem. Eng. J.* **2022**, *430*, 132882.

[90] Ye, J. J.; Rao, D. W.; Yan, X. H. CO_2 electrochemical reduction boosted by the regulated electronic properties of metalloporphyrins through tuning an atomic environment. *New J. Chem.* **2021**, *45*, 10664–10671.

[91] Han, S. G.; Ma, D. D.; Zhou, S. H.; Zhang, K. X.; Wei, W. B.; Du, Y. H.; Wu, X. T.; Xu, Q.; Zou, R. Q.; Zhu, Q. L. Fluorine-tuned single-atom catalysts with dense surface Ni-N_4 sites on ultrathin carbon nanosheets for efficient CO_2 electroreduction. *Appl. Catal. B Environ.* **2021**, *283*, 119591.

[92] Zheng, S. S.; Zuo, C. J.; Liang, X. H.; Li, S. N.; Pan, F. Valence state of transition metal center as an activity descriptor for CO_2 reduction on single atom catalysts. *J. Energy Chem.* **2021**, *56*, 444–448.

[93] Li, X. Q.; Duan, G. Y.; Chen, J. W.; Han, L. J.; Zhang, S. J.; Xu, B. H. Regulating electrochemical CO_2RR selectivity at industrial current densities by structuring copper@poly(ionic liquid) interface. *Appl. Catal. B Environ.* **2021**, *297*, 120471.

[94] Lee, J. H.; Park, I. K.; Duchesne, D.; Chen, L. S.; Lee, C. H.; Lee, J. H. Saline water electrolysis system with double-layered cation exchange membrane for low-energy consumption and its application for CO_2 mineralization. *J. CO_2 Utilizat.* **2020**, *41*, 101269.

[95] Chen, T. Y.; Hu, J.; Wang, K. Z.; Wang, K. J.; Zhang, W. J.; Gan, G. Y.; Shi, J. Effect of chloride adlayer on the oxide-derived gallium microspheres catalysts for electroreduction of CO_2 to CO. *J. Phys. Chem. Solids* **2022**, *163*, 110574.

[96] Lee, J. H.; Kattel, S.; Xie, Z. H.; Tackett, B. M.; Wang, J. J.; Liu, C. J.; Chen, J. G. Understanding the role of functional groups in polymeric binder for electrochemical carbon dioxide reduction on gold nanoparticles. *Adv. Funct. Mater.* **2018**, *28*, 1804762.

[97] Liu, J. Z.; Wang, Y. T.; Jiang, H.; Jiang, H. B.; Zhou, X. D.; Li, Y. H.; Li, C. Z. Ag@Au core-shell nanowires for nearly 100% CO_2-to-CO electroreduction. *Chem. Asian J.* **2020**, *15*, 425–431.

[98] Xia, Z.; Freeman, M.; Zhang, D. X.; Yang, B.; Lei, L. C.; Li, Z. J.; Hou, Y. Highly selective electrochemical conversion of CO_2 to HCOOH on dendritic indium foams. *ChemElectroChem* **2018**, *5*, 253–259.

[99] Bagger, A.; Arán-Ais, R. M.; Stenlid, J. H.; Dos Santos, E. C.; Arnarson, L.; Jensen, K. D.; Escudero-Escribano, M.; Cuenya, B. R.; Rossmeisl, J. *Ab initio* cyclic voltammetry on Cu(111), Cu(100) and Cu(110) in acidic, neutral and alkaline solutions. *ChemPhysChem* **2019**, *20*, 3096–3105.

[100] Kortlever, R.; Tan, K. H.; Kwon, Y.; Koper, M. T. M. Electrochemical carbon dioxide and bicarbonate reduction on copper in weakly alkaline media. *J. Solid State Electrochem*. **2013**, *17*, 1843–1849.
[101] Huang, Y.; Ong, C. W.; Yeo, B. S. Effects of electrolyte anions on the reduction of carbon dioxide to ethylene and ethanol on copper (100) and (111) surfaces. *ChemSusChem* **2018**, *11*, 3299–3306.
[102] Zhang, Q.; Shao, X. L.; Yi, J.; Liu, Y. Y.; Zhang, J. J. An experimental study of electroreduction of CO_2 to HCOOH on SnO_2/C in presence of alkali metal cations (Li^+, Na^+, K^+, Rb^+ and Cs^+) and anions (HCO_3^-, Cl^-, Br^- and I^-). *Chin. J. Chem. Eng*. **2020**, *28*, 2549–2554.
[103] Yoon, S. H.; Piao, G.; Park, H.; Elbashir, N. O.; Han, D. S. Theoretical insight into effect of cation-anion pairs on CO_2 reduction on bismuth electrocatalysts. *Appl. Surf. Sci*. **2020**, *532*, 147459.
[104] Zhang, Y. N.; Liu, L.; Shi, L.; Yang, T. T.; Niu, D. F.; Hu, S. Z.; Zhang, X. S. Enhancing CO_2 electroreduction on nanoporous silver electrode in the presence of halides. *Electrochim. Acta* **2019**, *313*, 561–569.
[105] Garg, S.; Li, M. R.; Wu, Y. M.; Idros, M. N.; Wang, H. M.; Yago, A. J.; Ge, L.; Wang, G. G. X.; Rufford, T. E. Understanding the effects of anion interactions with Ag electrodes on electrochemical CO_2 reduction in choline halide electrolytes. *ChemSusChem* **2021**, *14*, 2601–2611.
[106] Hong, S.; Lee, S.; Kim, S.; Lee, J. K.; Lee, J. Anion dependent CO/H_2 production ratio from CO_2 reduction on Au electro-catalyst. *Catal. Today* **2017**, *295*, 82–88.
[107] Ovalle, V. J.; Waegele, M. M. Impact of electrolyte anions on the adsorption of CO on Cu electrodes. *J. Phys. Chem. C* **2020**, *124*, 14713–14721.
[108] Cho, M.; Song, J. T.; Back, S.; Jung, Y.; Oh, J. The role of adsorbed CN and Cl on an Au electrode for electrochemical CO_2 reduction. *ACS Catal*. **2018**, *8*, 1178–1185.
[109] Ogura, K. Electrochemical reduction of carbon dioxide to ethylene: Mechanistic approach. *J. CO_2 Utilizat*. **2013**, *1*, 43–49.
[110] Ogura, K.; Ferrell, J. R.; Cugini, A. V.; Smotkin, E. S.; Salazar-Villalpando, M. D. CO_2 attraction by specifically adsorbed anions and subsequent accelerated electrochemical reduction. *Electrochim. Acta* **2010**, *56*, 381–386.
[111] Ogura, K.; Salazar-Villalpando, M. D. CO_2 electrochemical reduction via adsorbed halide anions. *JOM* **2011**, *63*, 35–38.
[112] Chen, T. Y.; Hu, J.; Wang, K. Z.; Wang, K. J.; Gan, G. Y.; Shi, J. Specifically adsorbed anions enhance CO_2 electrochemical reduction to CO over a gallium catalyst in organic electrolytes. *Energy Fuels* **2021**, *35*, 17784–17790.
[113] Schizodimou, A.; Kyriacou, G. Acceleration of the reduction of carbon dioxide in the presence of multivalent cations. *Electrochim. Acta* **2012**, *78*, 171–176.
[114] Varela, A. S.; Ju, W.; Reier, T.; Strasser, P. Tuning the catalytic activity and selectivity of Cu for CO_2 electroreduction in the presence of halides. *ACS Catal*. **2016**, *6*, 2136–2144.
[115] Wan, Q. Q.; He, Q. C.; Zhang, Y.; Zhang, L. H.; Li, J.; Hou, J. B.; Zhuang, X. D.; Ke, C. C.; Zhang, J. L. Boosting the faradaic efficiency for carbon dioxide to monoxide on a phthalocyanine cobalt based gas diffusion electrode to higher than 99% via microstructure regulation of catalyst layer. *Electrochim. Acta* **2021**, *392*, 139023.
[116] Verma, S.; Lu, X.; Ma, S. C.; Masel, R. I.; Kenis, P. J. A. The effect of electrolyte composition on the electroreduction of CO_2 to CO on Ag based gas diffusion electrodes. *Phys. Chem. Chem. Phys*. **2016**, *18*, 7075–7084.
[117] Shao, P.; Zhou, W.; Hong, Q. L.; Yi, L. C.; Zheng, L. R.; Wang, W. J.; Zhang, H. X.; Zhang, H. B.; Zhang, J. Synthesis of a boron-imidazolate framework nanosheet with dimer copper units for CO_2 electroreduction to ethylene. *Angew. Chem., Int. Ed*. **2021**, *60*, 16687–16692.
[118] Akhade, S. A.; McCrum, I. T.; Janik, M. J. The impact of specifically adsorbed ions on the copper-catalyzed electroreduction of CO_2. *J. Electrochem. Soc*. **2016**, *163*, F477–F484.
[119] Ahmad, N.; Wang, X. X.; Sun, P. X.; Chen, Y.; Rehman, F.; Xu, J.; Xu, X. Electrochemical CO_2 reduction to CO facilitated by MDEA-based deep eutectic solvent in aqueous solution. *Renew. Energy* **2021**, *177*, 23–33.
[120] Piao, G.; Yoon, S. H.; Han, D. S.; Park, H. Ion-enhanced conversion of CO_2 into formate on porous dendritic bismuth electrodes with high efficiency and durability. *ChemSusChem* **2020**, *13*, 698–706.
[121] Ge, R.; Dong, L. Y.; Hu, X.; Wu, Y. T.; He, L.; Hao, G. P.; Lu, A. H. Intensified coupled electrolysis of CO_2 and brine over electrocatalysts with ordered mesoporous transport channels. *Chem. Eng. J*. **2022**, *438*, 135500.
[122] Tan, X. Y.; Yu, C.; Song, X. D.; Zhao, C. T.; Cui, S.; Xu, H. Y.; Chang, J. W.; Guo, W.; Wang, Z.; Xie, Y. Y. et al. Toward an understanding of the enhanced CO_2 electroreduction in NaCl electrolyte over CoPc molecule-implanted graphitic carbon nitride catalyst. *Adv. Energy Mater*. **2021**, *11*, 2100075.
[123] Peng, C.; Yang, S. T.; Luo, G.; Yan, S.; Shakouri, M.; Zhang, J. B.; Chen, Y. S.; Li, W. H.; Wang, Z. Q.; Sham, T. K. et al. Surface co-modification of halide anions and potassium cations promotes high-rate CO_2-to-ethanol electrosynthesis. *Adv. Mater*. **2022**, *34*, 2204476.

Zebi Zhao is a jointly-trained Ph.D. candidate in Prof. Lum's Group and will receive his Ph.D. degree from School of Integrated Circuits at Beijing University of Posts and Telecommunications expectedly in 2024. His current research interests focused on novel and highly efficient electrocatalysts for CO_2 reduction reaction.

Jiguang Zhang is a Ph.D. student at the Agency for Science, Technology and Research (A*STAR) in Singapore. He received his BSc from Harbin Institute of Technology and MSc from Xiamen University. His current research focuses on electrochemistry, energy conversion materials and CO_2 reduction reaction.

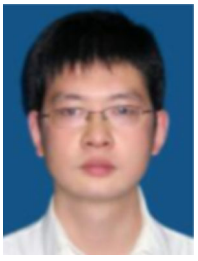

Prof. Ming Lei received his Ph.D. from the Laboratory of Nanophysics and Devices, Institute of Physics, Chinese Academy of Sciences in 2007. He worked as a postdoctoral fellow at The Hong Kong University of Science and Technology (2007−2008) and the Chinese University of Hong Kong (2009−2010). He is now a professor and doctoral supervisor at the School of Science, Beijing University of Posts and Telecommunications. He is now focusing on low-dimensional nanomaterials, photoelectric properties and device applications.

Yanwei Lum is a Research Scientist at the Agency for Science, Technology and Research (A*STAR) in Singapore. He received his BEng from Imperial College London and PhD from University of California, Berkeley. Prior to joining A*STAR, he was a PostDoctoral Fellow at the University of Toronto. Recent awards include the MIT TR35 Innovators Under 35 (Asia Pacific), ASEAN-ROK Next ASEAN Innovator Award and Singapore NRF Fellowship. His research interests include electrochemistry, materials chemistry, CO_2 conversion to chemicals/fuels and partial oxidation of hydrocarbon feedstocks.